

## Radar and lightning analyses of gigantic jet-producing storms

Tiffany C. Meyer,<sup>1,2</sup> Timothy J. Lang,<sup>1,3</sup> Steven A. Rutledge,<sup>1</sup> Walter A. Lyons,<sup>4</sup> Steven A. Cummer,<sup>5</sup> Gaopeng Lu,<sup>5</sup> and Daniel T. Lindsey<sup>6</sup>

Received 16 October 2012; revised 11 February 2013; accepted 25 February 2013.

[1] An analysis of thunderstorm environment, structure, and evolution associated with six gigantic jets (five negative polarity, one positive) was conducted. Three of these gigantic jets were observed within detection range of very high frequency lightning mapping networks. All six were within range of operational radars and two-dimensional lightning network coverage: five within the National Lightning Detection Network and one within the Global Lightning Detection (GLD360) network. Most of the storms producing the jets formed in moist tropical or tropical-like environments (precipitable water ranged from 37 to 62 kg m<sup>-2</sup>, and 0–6 km shear from 3.5 to 24.8 m s<sup>-1</sup>), featuring high convective available potential energy (1200–3500 J kg<sup>-1</sup>) and low lifted indices (–2.8 to –6.4). The storms had maximum radar reflectivity factors of 54 to 62 dBZ, and 10 dBZ echo contours reached 14–17 km. Storms covered by three-dimensional lightning mappers were near peak altitude of lightning activity (modes of the vertical distributions of radio sources were at altitudes colder than –50°C) and vertical reflectivity intensity, with overshooting echo tops around the times of their jets. Two of the other three jet-producing storms produced their jet around the time of a convective surge as indicated by radar data and likely featured overshooting tops. The observations suggest a link between convective surges, overshooting tops, and the occurrence of gigantic jets, similar to prior modeling studies.

**Citation:** Meyer, T. C., T. J. Lang, S. A. Rutledge, W. A. Lyons, S. A. Cummer, G. Lu, and D. T. Lindsey (2013), Radar and lightning analyses of gigantic jet-producing storms, *J. Geophys. Res. Atmos.*, 118, doi:10.1002/jgrd.50302.

### 1. Introduction

#### 1.1. Background

[2] All lightning—including cloud-to-ground (CG) and intracloud (IC) lightning, as well as the more uncommon transient luminous events (TLEs)—plays a role in the global electric circuit. Gigantic jets (GJs) are part of the TLE family. Like blue jets, they are thought to initiate from IC lightning and escape upward from cloud tops. GJs extend to higher altitude than blue jets, up to 70–90 km above mean sea level (MSL), and have a different appearance [Pasko and George, 2002; Su et al., 2003; Lyons et al., 2003]. Blue jets are thought to form via continuous positive leader-like propagation [Wescott et al., 1998; Wescott et al., 2001]. Gigantic jets have an impulsive re-brightening characteristic resembling negative leader processes [Pasko et al., 2002; Krehbiel et al., 2008].

[3] The first GJ was observed on 14 September 2001 by the Lidar Laboratory of Arecibo Observatory in Puerto Rico. The GJ reached ~70 km MSL off the northwest coast from the main core of a relatively small thunderstorm that had a cloud top of roughly 16 km [Pasko et al., 2002]. In July 2002, low-light-level cameras in Kenting, Taiwan, recorded five GJs above a 16 km tall thunderstorm over the South China Sea. The jets extended to heights ranging from 86 to 91 km [Su et al., 2003]. Two years later, a GJ was recorded in a frontal system over Anhui province of China, marking the first observation over land. A few months later, several jet-like TLEs were recorded over a thunderstorm on the coast of Guangdong province, China [Hsu et al., 2004]. Two low-light cameras near Marfa, Texas, recorded the first gigantic jet over North America on 13 May 2005. The likely parent thunderstorm was a high-precipitation supercell cluster with radar echo tops of at least 14 km. Since then, more GJs have been recorded in North America [van der Velde et al., 2007a, 2007b]. The first positive jet was observed just west of the island of Corsica in the Mediterranean Sea the night of 12 December 2009. A stationary Mediterranean winter thunderstorm with a cloud top of only 6.5 km produced this GJ. The positive polarity was confirmed by the electromagnetic waveforms observed at various radio receiver stations [van der Velde et al., 2010].

[4] In 2010, three GJs were optically detected in different storms within detection range of ground-based, very high frequency (VHF) networks that resolve three-dimensional (3D) lightning development. Lu et al. [2011b] examined two of these jets and indicated that lightning development

<sup>1</sup>Department of Atmospheric Science, Colorado State University, Fort Collins, Colorado, USA.

<sup>2</sup>Warning Decision Training Branch, National Weather Service, Norman, Oklahoma, USA.

<sup>3</sup>NASA Marshall Space Flight Center (ZP11), Huntsville, Alabama, USA.

<sup>4</sup>FMA Research, Inc, Fort Collins, Colorado, USA.

<sup>5</sup>Electrical and Computer Engineering Department, Duke University, Durham, North Carolina, USA.

<sup>6</sup>NOAA/NESDIS/STAR/RAMMB, Fort Collins, Colorado, USA.

Corresponding author: T. J. Lang, NASA Marshall Space Flight Center (ZP11), Huntsville, AL 35812, USA. (tjlangco@gmail.com)

associated with these negative GJs was remarkably similar in that both jets initiated from convective cells that were producing normal polarity IC lightning between mid-level negative and upper positive charge regions. The GJs were produced by lightning flashes that developed as if there were a depleted upper positive charge region, as suggested by *Krehbiel et al.* [2008]. Table 1 shows a list of ground-based GJs observed and some of the storm characteristics. Overall, at least 24 GJs have been recorded in storms with deep convection, consisting of >14 km echo tops and ~55 dBZ reflectivity cores. Continued observations are being taken to capture more GJs in hopes to better understand them.

## 1.2. Upward Lightning Formation

[5] The formation of CG and IC lightning is reasonably well understood; however, blue jet and gigantic jet formation processes are still not fully understood. *Krehbiel et al.* [2008] offered a hypothesis as to how upward electrical discharges develop from thunderstorms.

[6] As the storm charges and the electric fields build up from precipitation, discharges occur, producing different types of lightning. Normally, electrified storms tend to develop an overall negative charge imbalance with time, as a result of the negative screening charge flowing to the cloud top [*Wilson*, 1921]. A –CG discharge occurs when a breakdown is triggered between the mid-level negative and lower positive charges [*Marshall et al.*, 2005], thereby charging the global electric circuit. After a –CG discharge, the storm’s net charge becomes positive, and the electric field is enhanced in the upper part of the storm [*Wilson*, 1956]. As the storm continues to charge, a discharge can be triggered in the upper part of the storm that can escape upward. The upward discharge would have the same polarity as the

storm, namely positive for a normally electrified storm. These upward discharges are known as blue jets [*Krehbiel et al.*, 2008].

[7] *Krehbiel et al.* [2008] suggest a secondary mechanism for the formation of upward discharges. Bolt-from-the-blue (BFB) discharges are classic, bi-level IC flashes, with an upward negative leader that propagates into upper level positive charge. If that positive charge is depleted, the leader may exit the cloud and continue to the ground [*Rison et al.*, 1999]. As the BFB exits the cloud, it may be “guided” by inferred positive screening charge attracted to the lateral cloud boundaries by the mid-level negative charge [*Krehbiel et al.*, 2008]. In the case of a negative gigantic jet, there is no “guiding” so the preferred discharge mode of the IC flash with a depleted upper positive charge is upward. In a normal polarity thunderstorm, the negative GJ effectively discharges the mid-level negative storm charge.

[8] Blue jets contribute to charging of the global electric circuit, whereas negative GJs weaken the circuit [*Su et al.*, 2003]. For the case of an inverted electrified storm, with positive charge near mid-levels, a negative blue jet or positive gigantic jet may be produced instead. In this case, the positive GJ would contribute to the global circuit.

## 1.3. Overview of the Present Study

[9] Given the relative rarity of GJ observations, the meteorological context for their occurrence is not well known. Most GJs observed in past studies developed from intense, tall thunderstorms [*Pasko et al.*, 2002; *Su et al.*, 2003; *van der Velde et al.*, 2007a; *Soula et al.*, 2011]. A reasonable hypothesis is that intense thunderstorms undergoing convective surges may provide favorable characteristics for the development of GJs; as such, thunderstorms often feature turbulent mixing and overshooting tops that could disrupt

**Table 1.** Ground-Based Gigantic Jet Observations<sup>a</sup>

Date	Place	L/W	Storm Type	Cloud Top (km)	Jet Height (km)	Reference	Notes
15 Sep 2001	200 km NW of Puerto Rico	Water	Thunderstorm Cell	16	87-91	Pasko et al., 2002	
22 Jul 2002	~500 km SSW of Kenting, Taiwan	Water	Thunderstorm Cell	16	86-91	Su et al., 2003	5 events between 1409 and 1421 UTC
18 Jun 2004	~700 km from Anhui province of China	Land	Frontal System	?	?	Hsu et al., 2004	
3 Aug 2004	~500 km from Guandong province, China	Coast	Thunderstorm Cell	?	70	Hsu et al., 2004	Possible gigantic jet
13 May 2005	Northern Mexico	Land	High Precipitation Supercell	14	69-80	van der Velde et al., 2007a	
22 July 2007	Fujian Province, China	Land	Thunderstorm Cell	15	≥65	Chou et al. 2011	Originated as blue starter/jet
20 Aug 2007	Missouri	Land	Multicell Thunderstorm	15-16	94 & 83	van der Velde et al., 2007b	Produced 2 jets and a sprite
21 Jul 2008	Off coast near Duke	Water	Tropical Storm (TS) Cristobal	15	88	Cummer et al., 2009	
8 May 2009	Off coast near Duke	Water	Isolated cell				
12 Dec 2009	West of Corsica	Water	Stationary winter thunderstorm	6.5	91	Van der Velde et al., 2010	First + GJ produced ~50 TLEs
7 Mar 2010	East of Reunion Island	Water	Isolated tropical storm	?	80-90	Soula et al., 2011	5 events between 1740 and 1829 UTC
9 Sep 2010	Eastern OK	Land	TS Hermine	15	90	Lu et al., 2011b	2 events in 10 minutes
28 Sep 2010	205 km from Sebring, FL	Water	Convective Cell (Remnants of TS)	16.2	80	Lu et al., 2011b	First jet to ascend into daytime ionosphere
17 Apr 2011	NC	Water	Squall line supercell	15	?	Lu et al., 2011a	Positive GJ
22 Sep 2011	Puerto Rico	Land	Convective cell in a tropical airmass	15	?	Lyons (2012)* URSI talk	

<sup>a</sup>Highlighted in grey are the cases examined in this study.

the upper charge layers through depletion or displacement of the negative upper screening layer and the main upper positive charge region [Riousset *et al.*, 2010].

[10] Gigantic jets are far less common than convective surges and overshooting tops, so this should be thought of as a potentially necessary condition for GJ development rather than a sufficient one. The idea is that disruption of the upper charge regions through convective surges and overshooting tops make GJ occurrence more likely, rather than assuring their occurrence. Thus, GJs should be more common when storms are undergoing convective surges and during times when overshooting tops are present.

[11] In order to test this hypothesis, the meteorological contexts for six gigantic jets were examined. Three negative GJs occurred within 3D VHF lightning mapping networks: two in Oklahoma and one in Florida. Lu *et al.* [2011b] looked at one of the Oklahoma jets and the Florida GJ. A fourth negative GJ in Puerto Rico, a negative jet off the coast of North Carolina, and a positive jet also off the coast of North Carolina also were analyzed. The last three jets were not within 3D lightning mapping range, but two-dimensional (2D) lightning data were analyzed. An analysis of the meteorological environments and radar-observed storm structures was performed for all six GJs.

## 2. Data and Methodology

### 2.1. Overview

[12] Lightning, radar, and sounding data were used to analyze the storms producing gigantic jets in this study. Two different ground-based 2D lightning networks were used as well as two 3D VHF lightning mapping networks. For each storm, data from the closest radar were obtained, and the sounding profile at a time and location close to the jet was analyzed. Since the jets have only been recorded via low-light cameras at night, visible satellite data—critical for identifying overshooting tops—was not useful. However, infrared satellite imagery was examined.

### 2.2. Two-Dimensional Lightning Networks

#### 2.2.1. National Lightning Detection Network

[13] Vaisala's National Lightning Detection Network (NLDN) has been detecting the electromagnetic radiation from lightning return strokes and providing detailed lightning data for the entire continental United States since 1989 [Cummins *et al.*, 1998; Orville, 2008]. Up until 2006, only CG lightning flashes were reported by the NLDN; however, previous studies had shown that severe storms produce much higher rates of IC lightning than CG [MacGorman and Nielsen, 1991; Williams *et al.*, 1999; Wiens *et al.*, 2005]. Thus, in the early 2000s, NLDN sensors were modified to allow improved detection of large-amplitude, very low frequency/low frequency (VLF/LF) pulses by IC flashes [Cummins and Murphy, 2009]. Lightning information on location, amplitude (peak current), and polarity is recorded for each stroke within a flash (CG or IC). A flash is defined by Cummins and Murphy [2009] as the ensemble of all CG strokes that strike within 10 km of each other within a 1 s interval. The NLDN has a detection efficiency up to 95% and location accuracy <500 m for CG lightning, while IC flash detection efficiency is on the order of 25–30% [Cummins and Murphy, 2009].

#### 2.2.2. Global Lightning Dataset (GLD360)

[14] In 2009, Vaisala's Global Lightning Dataset (GLD360) was launched as a ground-based, lightning-detection network capable of providing worldwide coverage. The network consists of long-range VLF sensors and became fully operational in May 2011. GLD360 data have a 70% CG flash detection efficiency and a 5–10 km median CG stroke location accuracy [Demetriades *et al.*, 2010]. The network reports peak current ( $I_{pk}$ ) and polarity estimates but does not classify the strokes as CG or IC [Said *et al.*, 2010]; however, a classification of  $|I_{pk}| > 7$  kA and  $|I_{pk}| < 7$  kA for CGs and ICs, respectively [Holle, 2009], was used for identification in this study.

### 2.3. Three-Dimensional Lightning Mapping Networks

#### 2.3.1. Oklahoma Lightning Mapping Array

[15] The Lightning Mapping Array (LMA) was developed at the New Mexico Institute of Mining and Technology [Krehbiel *et al.*, 2000] and was modeled after the Lightning Detection and Ranging (LDAR) system developed for the Kennedy Space Center (KSC) [Maier *et al.*, 1995]. The LMA detects VHF radiation emitted by leaders during development of a lightning flash [Rison *et al.*, 1999]. The system is able to map total lightning activity, including IC and CG lightning, in all three spatial dimensions as a function of time. While 3D mapping is best done within 100 km range of network center, both the horizontal and altitude location data have proven to be scientifically useful even beyond 200 km range [MacGorman *et al.*, 2008; Lang *et al.*, 2010, 2011; Lu *et al.*, 2011b].

#### 2.3.2. Four-Dimensional Lightning Surveillance System

[16] The Four-Dimensional Lightning Surveillance System (4DLSS) represents an upgrade and merger of the LDAR system [Lennon and Maier, 1991] and the Cloud-to-Ground Lightning Surveillance System (CGLSS) [Boyd *et al.*, 2005] at KSC in Florida. The LDAR component consists of nine VHF antennas that sense impulsive emissions from lightning in the 60–66 MHz range [Roeder, 2010]. Similar to the Oklahoma LMA, the LDAR system detects IC lightning and produces a full 3D spatial mapping of lightning discharge activity. The CGLSS system uses similar sensors to the NLDN [Biagi *et al.*, 2007] to detect CG flashes [Murphy *et al.*, 2008].

### 2.4. Radar, Satellite, and Sounding Data

[17] For each storm, nearby NEXRAD Level II radar data were obtained from the [has.ncdc.noaa.gov](http://has.ncdc.noaa.gov) website. For all scans ranging from 30 min before to 30 min after the jet, the latitude and longitude points of a polygon that surrounded the entire storm which produced the jet were identified using the Warning Decision Support System-II (WDSS-II) software. The minimum box size used (Puerto Rico case) was approximately 20 km by 20 km, and the maximum size used was 20 km by 40 km (Oklahoma case). Focus was placed on only the core (or possible cores, if jet location was ambiguous) that produced the GJ, and on following that core as it moved by shifting the box location in time.

[18] Two different methods were used to interpolate the data to a grid. The first involved using the National Center for Atmospheric Research SPRINT radar data interpolation software. This software interpolates radar measurements taken in spherical coordinates and converts them to regularly

spaced latitude-longitude grids in height [Mohr and Vaughn, 1979]. When necessary to fill in missing data, the WDSS-II software was used. WDSS-II was developed by the National Severe Storms Laboratory to manipulate radar data [Lakshmanan et al., 2007; Hondl, 2003]. WDSS-II was used to input Level II WSR-88D data and create mosaic data from a single radar by transforming the data into latitude, longitude, and height grids [Lakshmanan et al., 2006]. The output for both of these methods was grids with reflectivity data at each  $0.01^\circ$  ( $\sim 1$  km) in the horizontal and 1 km in the vertical.

[19] Longwave infrared satellite imagery from the Geostationary Operational Environmental Satellites (GOES) was examined for each of the cases, around the times of the jets. Locations of GJs were compared to the locations of the coldest cloud tops. Atmospheric sounding data were taken from the closest site. The temperature and dewpoint vertical profiles were looked at as well as convective available potential energy (CAPE), lifted index (LI), and wind shear values.

### 3. Gigantic Jet Cases

[20] The GJ observations are reported below by the geographic location in which they occurred. Two GJs occurred in Oklahoma, one in Florida, one in Puerto Rico, and two offshore near North Carolina. Each case is summarized by observations, environmental conditions, and discussion. These include where and when the jet occurred, the atmospheric soundings around the time of the jet, the evolution of the storm, and radar and electric structure via cross-sections, contoured frequency by altitude diagrams, and time series plots.

#### 3.1. Oklahoma

##### 3.1.1. Overview

[21] Two negative GJs were recorded in eastern Oklahoma on 9 September 2010 at 7:22 UTC and 7:28 UTC, respectively. The GJs were observed from Hawley, Texas ( $32.66^\circ\text{N}$ ,  $99.84^\circ\text{W}$ ) from a Watec 902H2 camera stamped with exact Global Positioning System time  $\sim 500$  km away from the storm, and GJ locations were fixed via querying the Oklahoma LMA data near the times of the GJs [Lu et al., 2011b]. A negative sprite also was observed at 6:49 UTC in this storm [Lu et al., 2012], though not examined in this study. The GJs were within 225 km of the center of the Oklahoma LMA [MacGorman et al., 2008]. This is a little far for optimal 3D mapping, but the upper lightning structure was still resolved. Two-dimensional NLDN data also were available for this storm.

##### 3.1.2. Environment

[22] The storm producing the two negative jets was a strong thunderstorm embedded in the remnants of Tropical Storm Hermine. Hermine developed off the coast of southeastern Mexico five days prior to the jet observations. Many tornado, wind, and flooding reports were recorded throughout Texas and Oklahoma as Hermine made its way inland (reports may be found at <http://www.spc.ncep.noaa.gov/exper/archive/events/searchindex.html>). Hermine was still considered a tropical depression when the GJ-producing storm formed. The environment was very moist and tropical-like. The 0 UTC sounding from Norman, Oklahoma, was examined. The sounding showed melting and tropopause heights of 5.1 and 15.7 km, respectively (Table 2). The CAPE value was  $45 \text{ J kg}^{-1}$ , and the LI was 0.3, indicative

of a moist neutral air mass. The 0–6 km wind shear was strong, over  $15 \text{ m s}^{-1}$ , and precipitable water was  $61.8 \text{ kg m}^{-2}$ . The 12 UTC sounding was similar to the 0 UTC sounding, but slightly drier aloft. Surface and upper air plots showed southwesterly flow in north Texas and southern Oklahoma, and the 0 UTC sounding from Dallas contained considerably more CAPE and more negative LI ( $\sim 2300 \text{ J kg}^{-1}$  and  $-3.1$ , respectively). Thus, it is possible that significantly more unstable air was being advected into the region of the storm, helping to fuel the convection. These Dallas stability values are thus considered more representative and are reported for this storm in Table 2. The GJ storm moved  $\sim 16 \text{ m s}^{-1}$  toward the northeast.

##### 3.1.3. Results

[23] A vertical cross-section through the area of the first GJ was produced. Also overlaid are the LMA lightning source data contoured in  $\sim 1 \text{ km}^2$  bins (Figure 1). A lightning source maximum was located around the area of the first GJ. The bulge in reflectivity at the storm top was an overshooting top extending through the local tropopause. The maximum reflectivity in this storm was 54 dBZ at 2 km, 8 min before the first jet formed. The 10 dBZ echo top was at an altitude of  $\sim 15.5$  km MSL.

[24] Figure 2 shows the relationship between GOES infrared (IR) brightness temperatures and jet locations, around the times of the jets. The jets occurred in close proximity to the coldest cloud tops (which were colder than  $-70^\circ\text{C}$ ). These cloud tops likely indicated the presence of overshooting tops near the jets. Based on qualitative analysis of the satellite data, the storm's anvil expanded horizontally at a roughly constant rate during the analysis period.

[25] Contoured frequency by altitude diagrams (CFADs) [Yuter and Houze, 1995] for the Oklahoma storm were constructed and overlaid with LMA altitude histograms (Figure 3). CFADs, which essentially show the probability distribution of radar reflectivity as a function of altitude, are useful for detecting important changes in storm structure such as convective surges and overshooting tops. The temporal period for data integration in each Figure 3 subplot was the duration of the radar volume scan ( $\sim 4.5$  min). Through the times of the two GJs, there was a large maximum in lightning source frequency near the  $-50^\circ\text{C}$  isotherm, indicating prolific IC activity and storm intensification. There was also a greater frequency of high reflectivity values (e.g.,  $>30$  dBZ) near  $-50^\circ\text{C}$ . This suggested a strong updraft lofting ice particles to high altitudes. After the two jets, the storm weakened, indicated by a decrease in lightning sources and the reduced frequency of significant reflectivity at middle and upper levels. The frequency in low-level, high reflectivity values increased at this point as well, indicating that large, precipitation-sized particles were falling out.

[26] Time series plots of lightning and reflectivity frequency also show the presence of a convective surge prior to the GJs. Figure 4a shows a peak of  $>30$  dBZ frequency just before the first jet, which continued through the time of the second jet, then decreased. A time series of the VHF source frequency from the LMA showed a general increase in the number and modal height of VHF sources above 10 km prior to the jets (Figure 4b). After the jets occurred, there was a dip in the lightning source frequency in the upper levels.

[27] The NLDN time series show the storm was producing mostly IC lightning (Figure 5). Very little CG lightning was

**Table 2.** Characteristics of the GJ Cases Examined in This Study

Date	Time (UTC)	Jet Type	Overshooting Top?	Time of Max Refl (UTC)	Max Refl (dBZ)	0–6 km Shear (m s <sup>-1</sup> )	CAPE (J kg <sup>-1</sup> )	LI	Precipitable Water (kg m <sup>-2</sup> )	Tropopause Height (km MSL)	Melting Level (km MSL)	10 dBZ Gridded Echo Top (km MSL)
9 Sep 2010	7:22:00	NGJ	Yes	7:14:48	54	15.3	2344	-3.1	61.8	15.7	5.1	16
28 Sep 2010	7:28:20	NGJ	Yes	10:41:03	59	3.5	2473	-4.8	51.9	16.7	4.9	17
22 Sep 2011	11:01:20	NGJ	Yes	5:23:32	57	3.8	3500	-6.0	54.9	14.6	5.0	15
8 May 2009	5:27:06	NGJ	Maybe	7:53:41	62	11.4	1207	-2.8	42.3	12.6	3.6	14
17 Apr 2011	8:08:02	NGJ	No	2:39:33	62	24.8	2298	-6.4	36.6	12.9	3.8	16
	3:11:28	PGJ	Yes									

NGJ is negative GJ; PGJ is positive GJ.

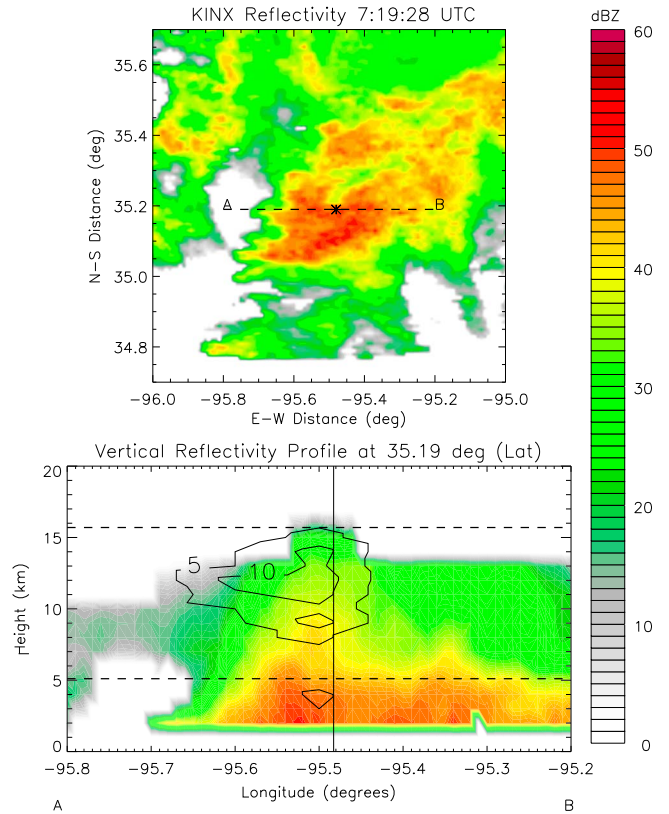


**Figure 1.** Plan view of KINX radar reflectivity data at the time of the first Oklahoma GJ (top). The dotted line represents the area of the vertical cross-section (bottom), with the GJ marked by the black asterisk (top). The vertical cross-section shows the melting level and tropopause heights (horizontal lines), jet location (vertical line), and overshooting top. Contoured in black is the OK-LMA lightning source density (sources per kilometer in the vertical and 0.01° in the horizontal).

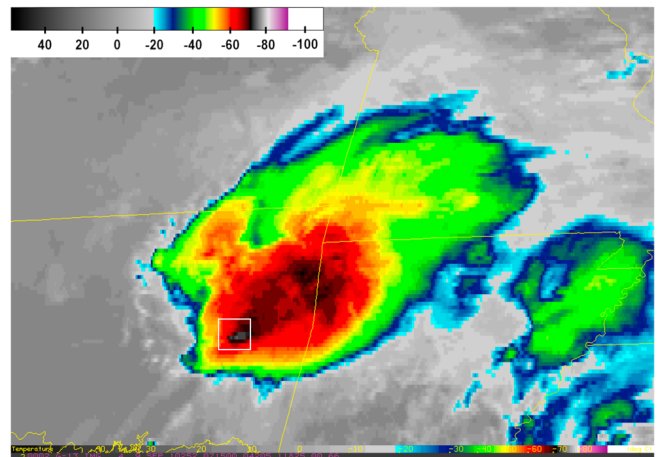


**Figure 2.** Infrared image of the Oklahoma GJ storm at 0715 UTC on 9 September 2010. Plotted are channel 4 (longwave infrared) brightness temperatures from the GOES-13 satellite. The locations of the GJs are centered within the white box, near the coldest cloud tops in the storm.

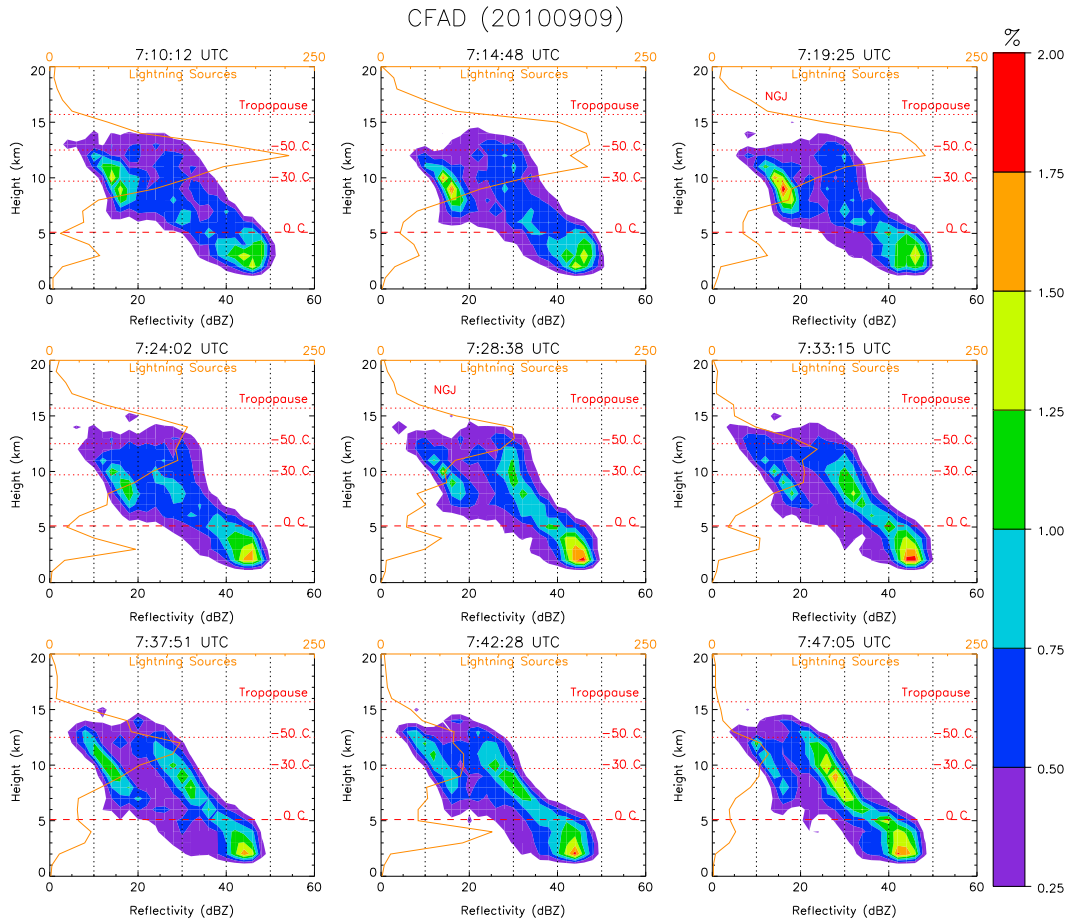


**Figure 3.** Contoured frequency by altitude diagrams (CFADs) showing the normalized distribution of reflectivity in 5 min bins versus height for nine time steps around the times of the Oklahoma jets. “NGJ” is labeled in the diagrams when the negative jets occurred. The lightning source frequency is plotted over 1 km levels in orange. Isotherms are plotted in red dashed lines.

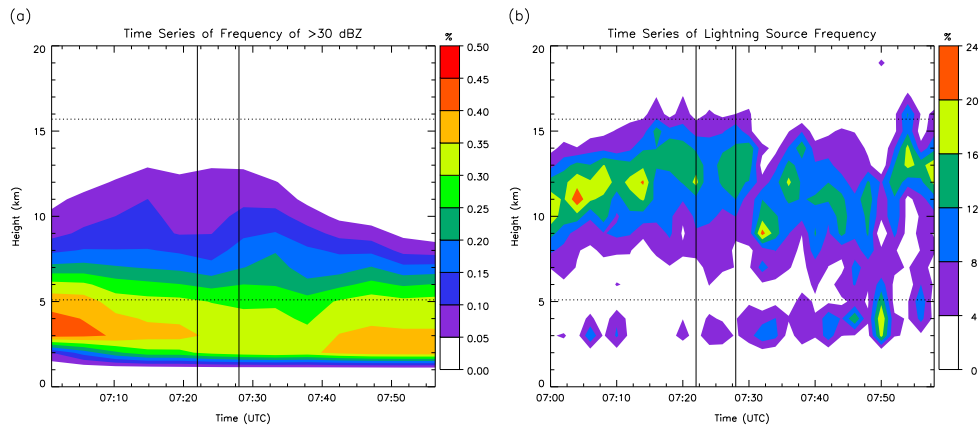


**Figure 4.** (a) Time series plots of the frequency of >30 dBZ versus height in 1 km levels with the Oklahoma jet times denoted by the black vertical lines. Also shown are horizontal lines indicating the freezing level altitude and the tropopause height. (b) Time series of the normalized three-dimensional VHF source frequency versus height.

present in the 20 min period prior to the first jet occurrence. The cumulative number of NLDN-detected IC lightning flashes/strokes increased significantly both before and

during the GJ time period, but leveled off afterward. Negative CG lightning began to pick up during the GJ period, but the sharpest increase occurred after the GJs. The overall

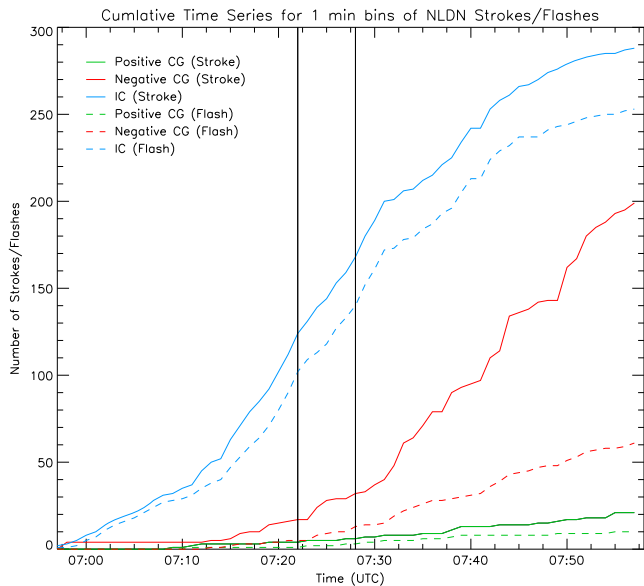


**Figure 5.** Cumulative time series plot of NLDN-detected flashes and strokes in 1 min bins for the Oklahoma jet storm. Positive CGs (green), negative CGs (red), and ICs (blue) are plotted with the time of the GJs (vertical lines).

results were consistent with storm intensification beginning prior to the occurrence of the GJs.

### 3.2. Florida

#### 3.2.1. Overview

[28] On 28 September 2010, another negative GJ was recorded in Sebring, Florida (27.52°N, 81.52°W). A Watco 902H2 camera was used to capture the jet, the same type used in the Oklahoma case. The GJ occurred off the east coast of Florida at 11:01 UTC  $\sim$ 70 km north of the 4DLSS. Its location was fixed via query of the 4DLSS data near the time of the GJ [Lu *et al.*, 2011b]. This storm also was well within detection range of the NLDN.

#### 3.2.2. Environment

[29] The sounding (Table 2) was taken from Tampa (KTWB) at 12 UTC, an hour after the jet occurred. The melting level was similar to the Oklahoma case at 4.9 km. However, the tropopause was about 1 km higher at 16.7 km, and the CAPE values were  $\sim$ 2500 J kg<sup>-1</sup> with an LI of  $-4.8$ . Wind shear was much weaker than the Oklahoma storm, but precipitable water was over 50 kg m<sup>-2</sup>. This indicated a very moist, unstable air mass with tropical characteristics. The GJ storm moved  $\sim$ 8 m s<sup>-1</sup> toward the north-northeast.

#### 3.2.3. Results

[30] A plan view of reflectivity data near the surface and a vertical cross-section with 4DLSS sources is shown in Figure 6. The jet-producing storm formed within a cluster of other storms. The storm structure was very similar to the Oklahoma case. The lightning maximum was concentrated in an overshooting top region; however, the overshooting top in this case did not penetrate the tropopause, according to the sounding (Table 2). This storm reached a peak reflectivity of 59 dBZ 20 min before the GJ. At the time

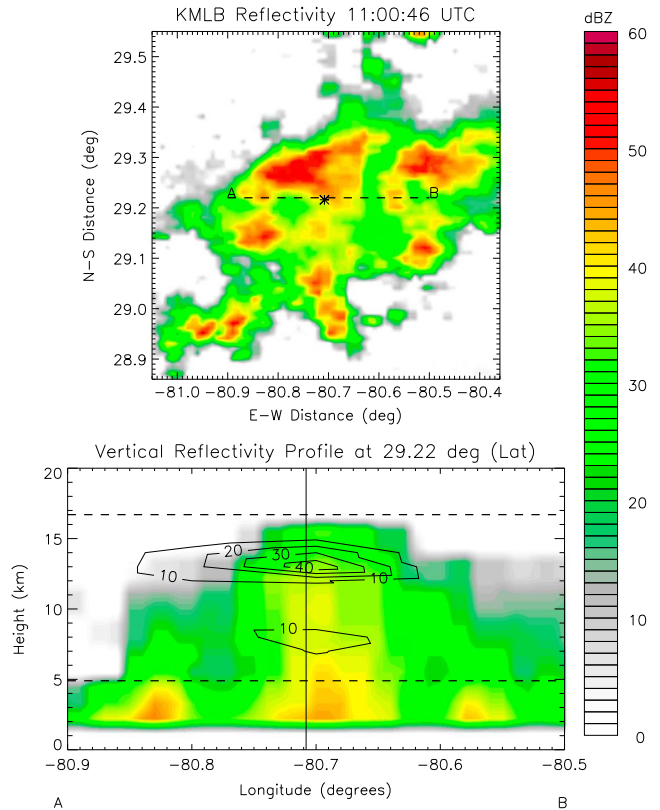


**Figure 6.** Plan view of KMLB radar reflectivity data at the time of the Florida GJ (top). The dotted line represents the area of the vertical cross-section (bottom), with the GJ marked by a black asterisk. The vertical cross-section shows the melting level and tropopause heights (horizontal lines), jet location (vertical line), and overshooting top. Contoured in black is the 4DLSS lightning source density (sources per kilometer in the vertical and 0.01° in the horizontal).

of the jet, there was a maximum reflectivity of 53 dBZ with 10 dBZ echo tops near 14 km MSL.

[31] The GOES satellite imagery indicated that the jet occurred very near the coldest cloud tops in the storm itself (Figure 7). However, those tops (about  $-60^{\circ}\text{C}$ ) were warmer than the clouds observed in the Oklahoma case and interestingly were not even the coldest tops in the region where the Florida storm occurred. However, there were indications of overshooting tops in the GJ storm at this and other times. Based on qualitative analysis of the satellite data, the storm's anvil expanded horizontally at a roughly constant rate during the analysis period.

[32] The CFAD for the Florida case showed an intensification of the storm leading up to the jet and a weakening of the storm after the jet (Figure 8). Reflectivity values of 35 dBZ reached 14 km just before the time of the jet. The peak lightning sources were around the  $-50^{\circ}\text{C}$  isotherm with the strongest peak at 13 km 5 min after the GJ.

[33] A time series plot for reflectivity values over 30 dBZ was produced for 30 min before and after the jet (Figure 9). The altitude of 30 dBZ or greater reflectivity peaked just before the time of the jet. At the 0–4 km region, there is a minimum in reflectivity frequency around the time of the jet. This may possibly indicate the presence of a strong updraft

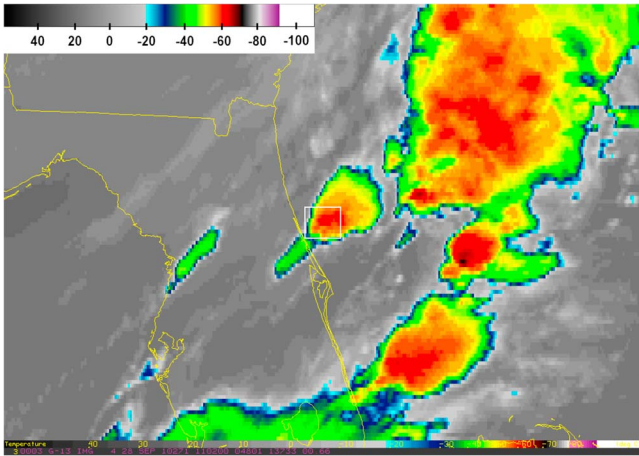


**Figure 7.** Infrared image of the Florida GJ storm at 1100 UTC on 28 September 2010. Plotted are channel 4 (longwave infrared) brightness temperatures from the GOES-13 satellite. The location of the GJ is centered within the white box, near the coldest cloud tops in the storm.

lifting particles upward [MacGorman *et al.*, 1989]. A lightning frequency time series plot was produced as well using the 4DLSS data (Figure 9). A clear lightning maximum near 13 km was present during and immediately after the time of

the jet, while at other times, the mode of the source distribution was shifted notably downward in altitude.

[34] The NLDN data are plotted as a function of time in Figure 10. Even accounting for the expected low detection efficiency of IC lightning by the NLDN, the storm was dominated by IC lightning and produced more negative CGs than positive CGs. Like the Oklahoma case, this storm produced few CGs leading up to the jet and a significant increase in negative CGs after the GJ. The rapid increase in IC lightning and the relative absence of CG lightning leading up to the jet suggest the storm was intensifying.

### 3.3. Puerto Rico

#### 3.3.1. Overview

[35] On 22 September 2011, another negative GJ was recorded with a Kodak Z749 digital camera on a tripod with a time stamp of 5:27 UTC from eastern Puerto Rico (18.05°N, 67.11°W). The jet was in the middle of the island along a 68° azimuth from the camera location (determined via photogrammetry), but the exact location of the GJ could not be pinpointed so analysis was performed for the nearest two cells along the azimuth line. Puerto Rico is outside NLDN range; thus, the GLD360 data were used.

#### 3.3.2. Environment

[36] The sounding was taken from San Juan, Puerto Rico, at 0 UTC, about 5.5 h before the jet (Table 2). The melting

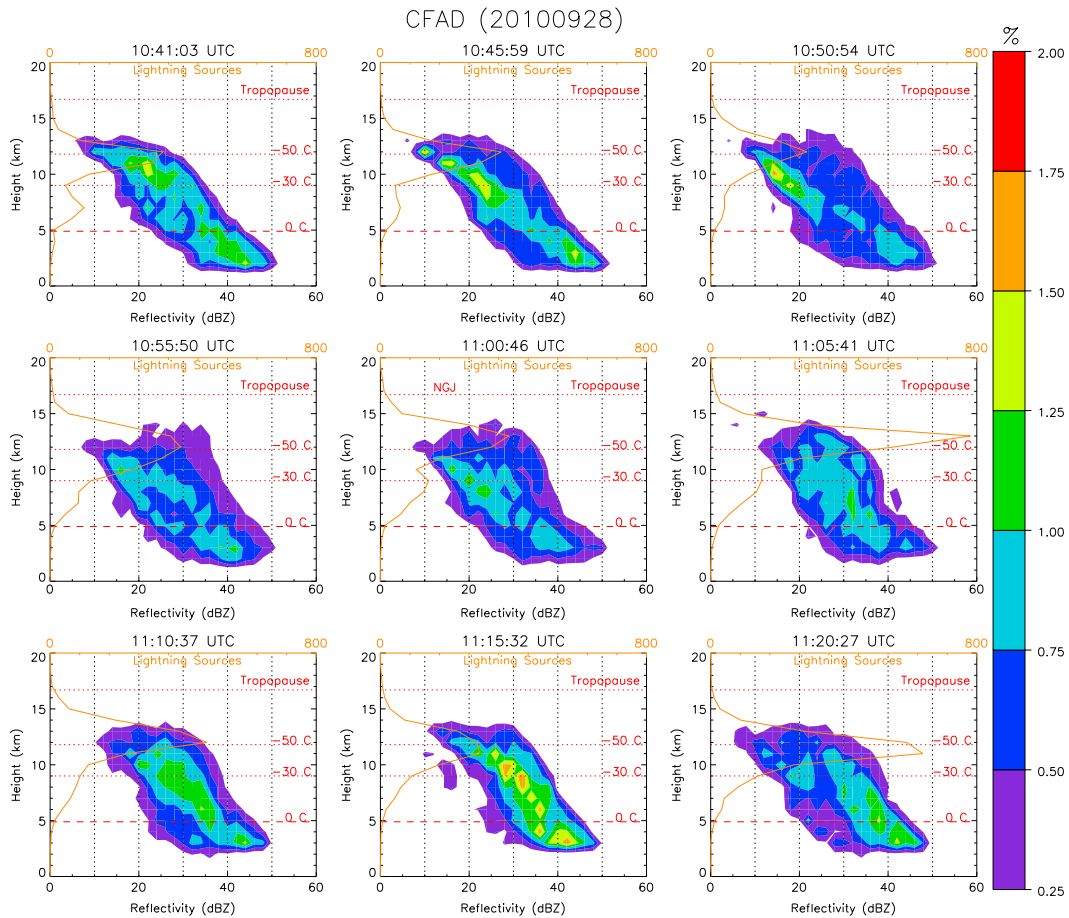


**Figure 8.** CFAD plots showing the normalized distribution of reflectivity in 5 min bins versus height for nine time steps around the time of the Florida jet. “NGJ” is labeled in the diagram when the jet occurred. The lightning source frequency is plotted over 1 km levels in orange. Isotherms are plotted in red dashed lines.

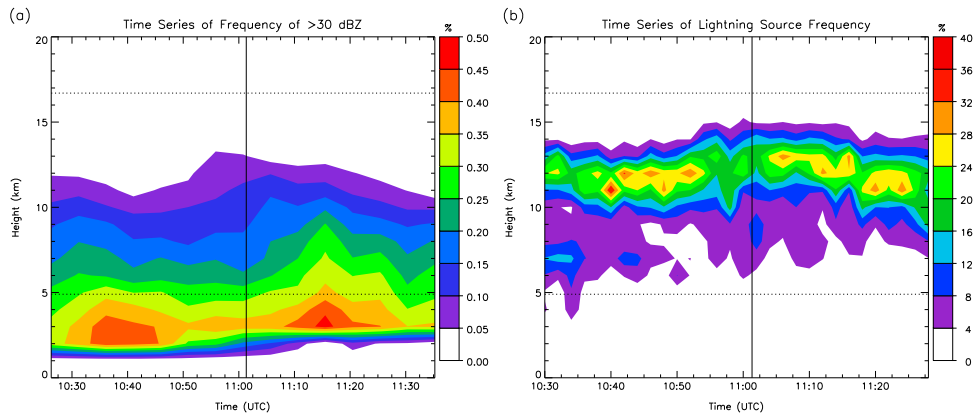


**Figure 9.** (a) Time series plots of the frequency of >30 dBZ versus height in 1 km levels with the Florida jet time denoted by the black vertical line. Also shown are horizontal lines indicating the freezing level altitude and the tropopause height. (b) Time series of the normalized three-dimensional VHF source frequency versus height.

level was the same as the previous cases at 5.0 km, and the tropopause height was a little bit lower at 14.6 km. The CAPE value was  $3500 \text{ J kg}^{-1}$  with an LI of  $-6.0$ . Wind shear was weak, comparable to the Florida case. Precipitable water was  $54.9 \text{ kg m}^{-2}$ . Overall, the environment featured tropical characteristics and was favorable for strong thunderstorms. The GJ storm moved toward the west-southwest at  $\sim 14 \text{ m s}^{-1}$ .

### 3.3.3. Results

[37] As stated before, the specific cell that produced the Puerto Rico jet could not be uniquely identified, and 3D lightning mapping observations were not available for analysis; however, the storm structure could still be analyzed with radar observations. The two storms in the vicinity of the jet were the strongest cells in the area. A cross-section was drawn through both possible cells (A and B; Figure 11),

along the approximate camera viewing azimuth, and the cell closer to the camera appeared to have a small overshooting top similar to the other cases. The storm farther from the camera did not have an overshooting top. The maximum reflectivity was 57 dBZ 5 min prior to the jet, with an echo top height of 15 km MSL, again similar to the Oklahoma and Florida cases. The ambiguity in position precluded directly associating the jet with the coldest cloud tops in

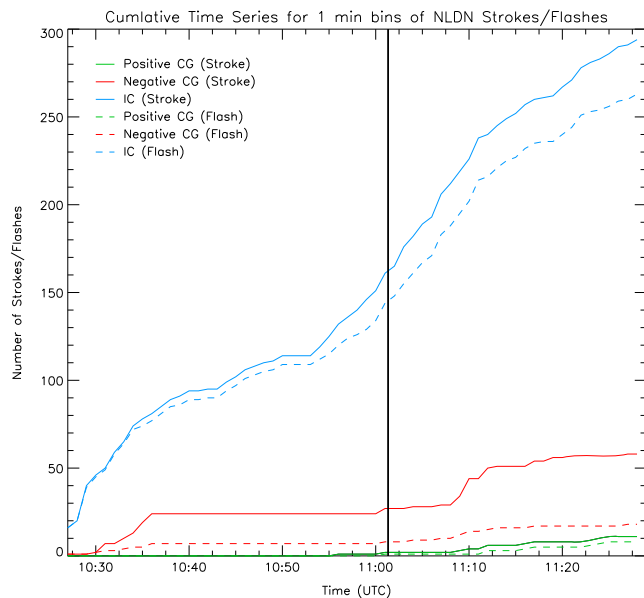


**Figure 10.** Cumulative time series plot for NLDN-detected flashes and strokes in 1 min bins. Positive CGs (green), negative CGs (red), and ICs (blue) are plotted with the time of the GJ (vertical line).

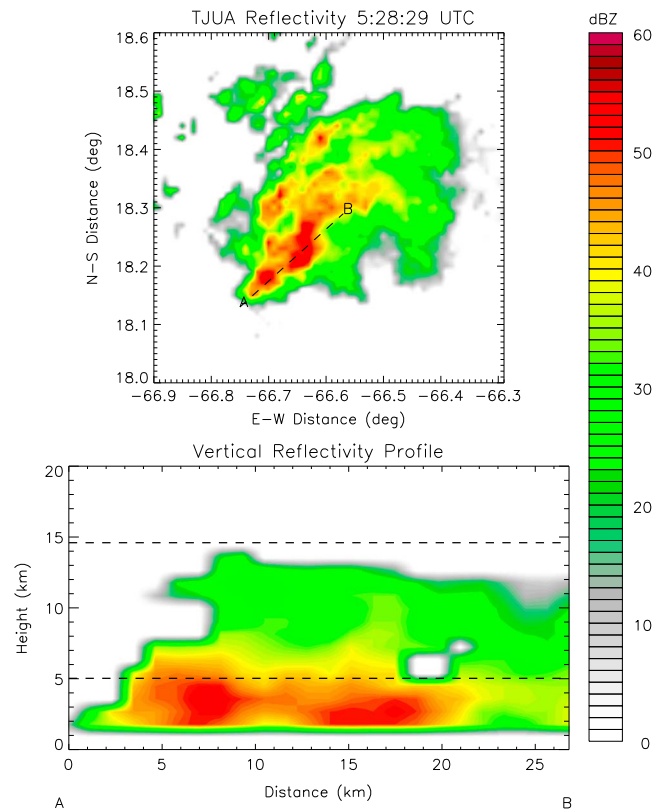


**Figure 11.** Plan view of TJUA radar reflectivity data at the time of the Puerto Rico GJ (top). The dotted line represents the area of the vertical cross-section (bottom). The vertical cross-section shows the melting level and tropopause heights (horizontal lines).

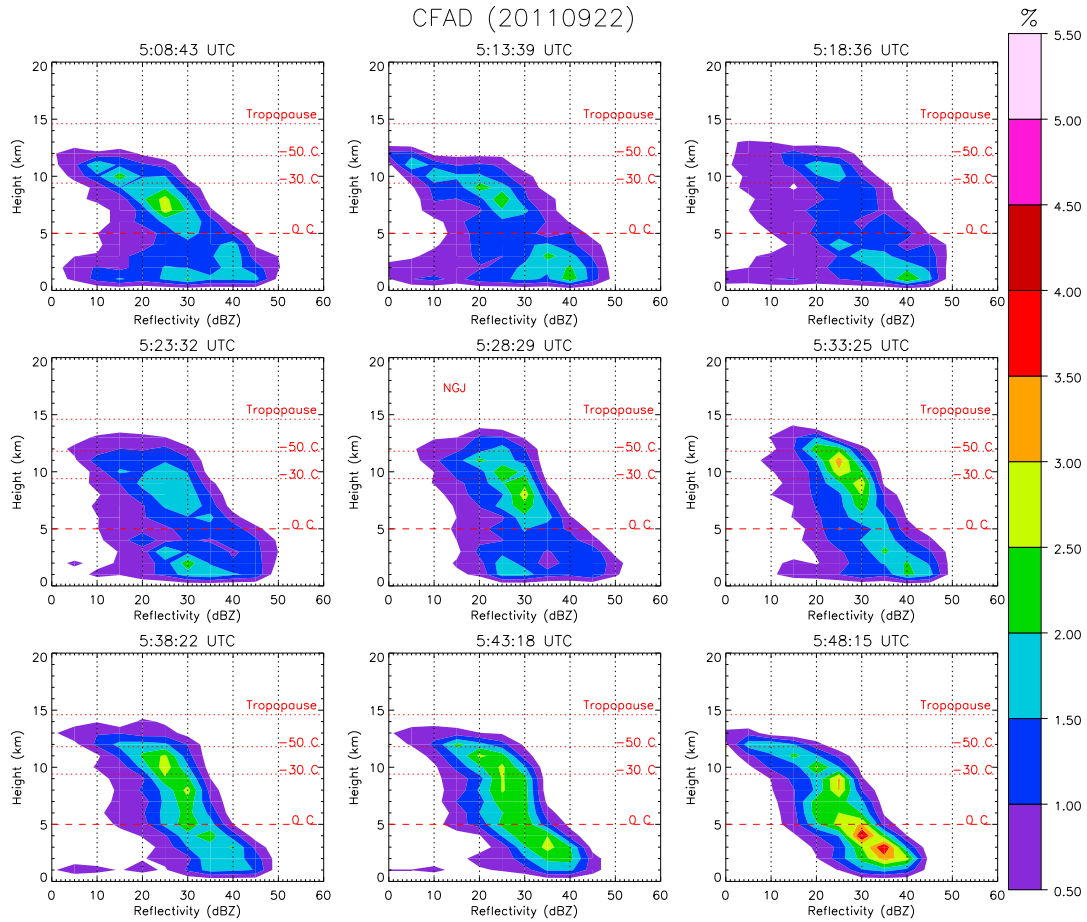


**Figure 12.** CFAD plots showing the normalized distribution of reflectivity in 5 min bins versus height for nine time steps around the time of the Puerto Rico jet. “NGJ” is labeled in the diagram when the jet occurred.

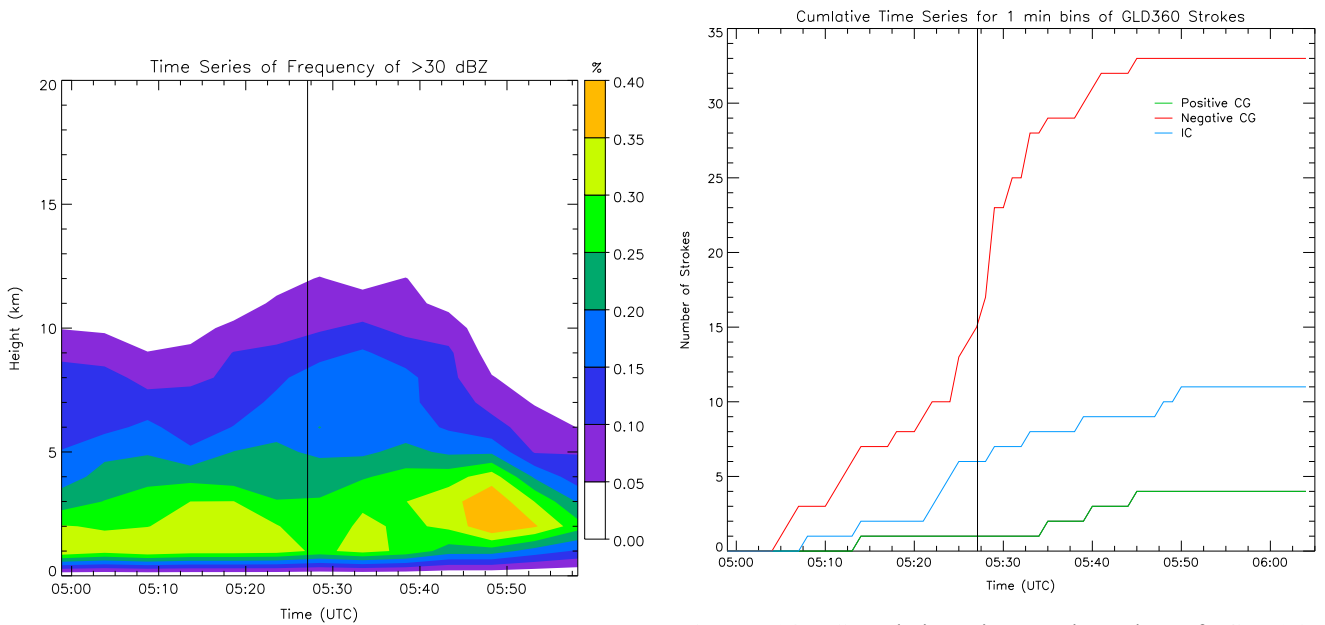


**Figure 13.** Time series plot of the frequency of >30 dBZ versus height in 1 km levels with the Puerto Rico jet time denoted by the black vertical line.

**Figure 14.** Cumulative time series plot of GLD360 lightning strokes in 1 min bins for the Puerto Rico jet storm. Positive CGs (green), negative CGs (red), and ICs (blue) are plotted with the time of the GJ (vertical line).

the storm. However, infrared satellite imagery (not shown) showed that the storm featured cloud-top brightness temperatures near  $-65^{\circ}\text{C}$ . Around the time of the GJ, the storm was undergoing a broad minimum in cloud-top temperature with possible indications of overshooting tops. Based on qualitative analysis of the satellite data, the storm's anvil expanded horizontally at a roughly constant rate during the analysis period.

[38] Like the previous cases, CFADs were produced; however, only reflectivity frequency was plotted since 3D lightning data were unavailable (Figure 12). Reflectivity data for both possible cells were included in the analysis since they were less than 5 km apart. An increase in 20–30 dBZ frequencies pushed through the tropopause height leading up to the time of the jet. The 5 min period after the jet occurred featured the peak frequency of 25 dBZ in the upper levels, indicating the storm was at its peak intensity. The next few scans showed that the maximum in the upper level reflectivity values started to shrink, and the frequency of the 30 dBZ increased near the lower levels, suggesting the larger hydrometeors were falling out.

[39] The time series reflectivity plot was consistent with the CFADs (Figure 13). A broad peak height of  $>30$  dBZ frequencies occurred during and after the time of the jet. Similar to the Oklahoma and Florida cases, there was a minimum frequency of  $>30$  dBZ in the lower layers, suggesting

the particles were being lifted by a strong updraft around this time.

[40] Figure 14 shows a limited number of strokes detected by the GLD360. This was due in part to a lower flash detection efficiency and larger uncertainty in location accuracy than NLDN [Demetriades *et al.*, 2010]. Overall, the storm was  $-CG$  dominant with an increase in strokes before and during the time of the jet, in contrast to the Oklahoma and Florida cases. Flash data were not available, however, and it is possible that a small number of high-multiplicity negative CG flashes accounted for the increase in cumulative stroke rate.

### 3.4. North Carolina

#### 3.4.1. Overview

[41] Two GJs have been recorded off the coast of North Carolina since 2009, one being negative and another being positive. The negative jet was recorded on 8 May 2009 at 8:08 UTC. The positive jet was observed on 17 April 2011 at 3:11 UTC. Both of these GJs were recorded by a WATEC 902H2 camera coupled to a triggered video acquisition system that records approximately 1 s of video when specified criteria are met. This camera is located in a field near Duke University ( $35.975^{\circ}\text{N}$ ,  $79.100^{\circ}\text{W}$ ) [Cummer *et al.*, 2009]. The exact position of the negative GJ could not be pinpointed, but it was seen along a  $117^{\circ}$ – $118^{\circ}$  azimuth from

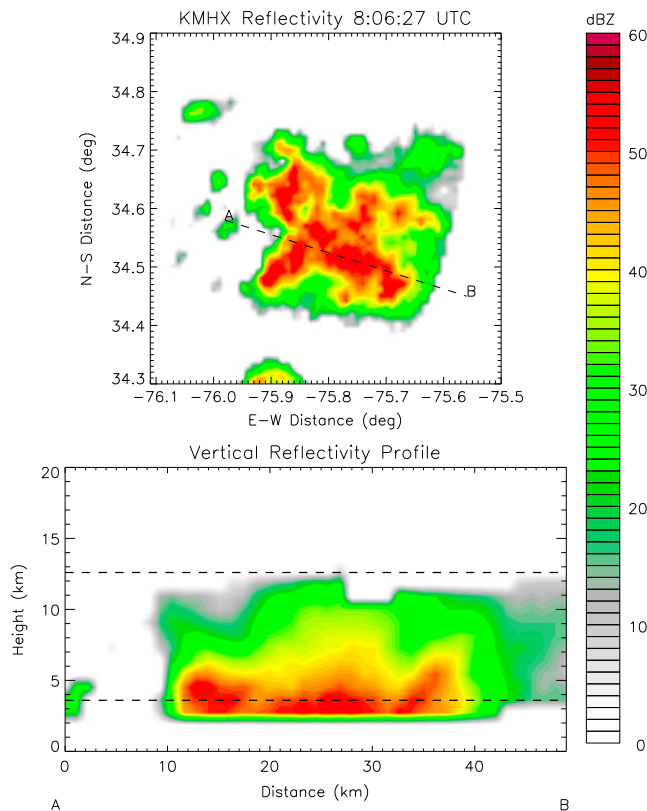


**Figure 15.** Plan view of KMHX radar reflectivity data at the time of the North Carolina negative GJ (top). The dotted line represents the area of the vertical cross-section (bottom). The vertical cross-section shows the melting level and tropopause heights (horizontal lines).

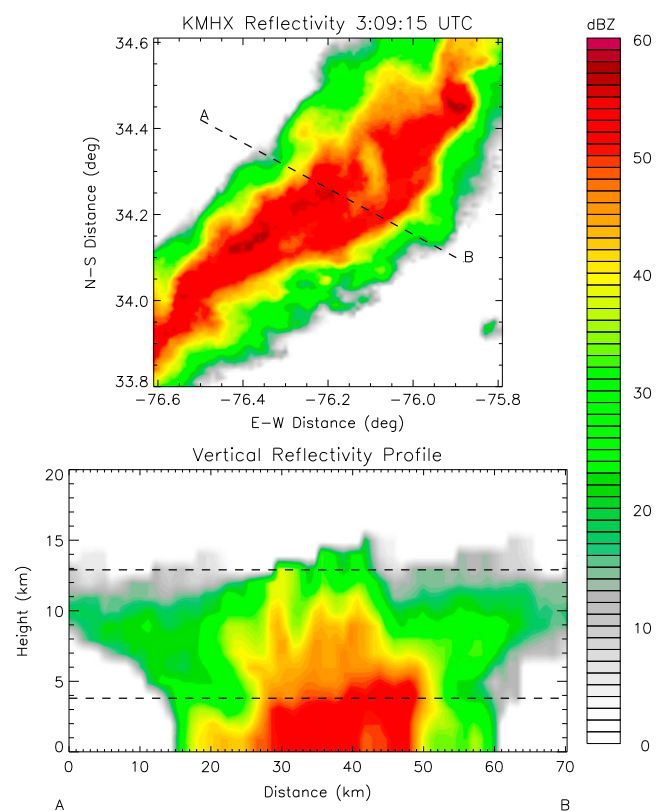


**Figure 16.** Plan view of KMHX radar reflectivity data at the time of the North Carolina positive GJ (top). The dotted line represents the area of the vertical cross-section (bottom), along the azimuth of the observed GJ. The vertical cross-section shows the melting level and tropopause heights (horizontal lines).

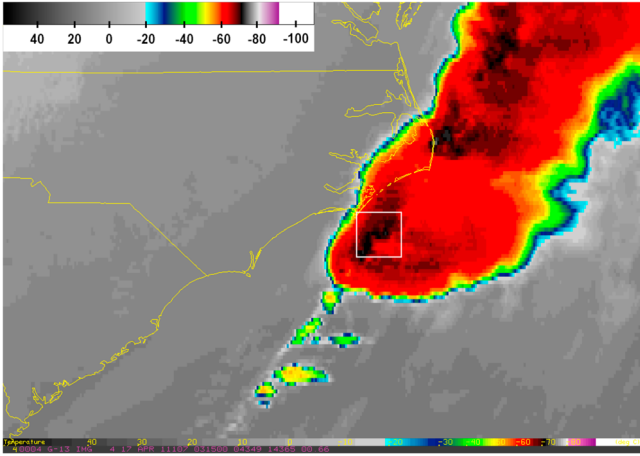


**Figure 17.** Infrared image of the North Carolina positive GJ storm at 0315 UTC on 11 April 2011. Plotted are channel 4 (longwave infrared) brightness temperatures from the GOES-13 satellite. The most likely location of the GJ is within the white box, near the coldest cloud tops in the storm.

the camera (determined via photogrammetry). The positive GJ occurred along an azimuth of  $125^{\circ}$ – $126^{\circ}$  from the camera (determined via photogrammetry), in a squall line off the

coast of North Carolina [Lu et al., 2011a]. Based on an average position of a group of negative CGs that occurred approximately 1 s before the positive GJ, its likely position was somewhere near  $34.23^{\circ}\text{N}$ ,  $76.21^{\circ}\text{W}$ . Like the Puerto Rico case, there were no VHF lightning mapping networks in the area; however, both of these GJ-producing storms were within NLDN range. The KMHX radar in Morehead, North Carolina, was used to analyze the reflectivity data.

**3.4.2. Environment**

[42] The soundings for both North Carolina cases were taken from Morehead City, North Carolina (Table 2). The 2009 negative GJ sounding at 0 UTC on 8 May showed melting level and tropopause heights at 3.6 and 12.6 km, respectively. This was lower than the other GJ cases, likely due to the springtime occurrence of the storm. The CAPE value was  $\sim 1200 \text{ J kg}^{-1}$ , and the LI was  $-2.8$ . Wind shear was over  $10 \text{ m s}^{-1}$ , while precipitable water also was  $42.3 \text{ kg m}^{-2}$ . The atmosphere was thus drier and more stable than the other cases, though it was still typical of tropical environments [Zveryaev and Chu, 2003]. The 12 UTC sounding from this day was even drier and more stable than the 0 UTC one; however, the later sounding was affected by the passage of the storm as it moved offshore, toward the east at  $\sim 20 \text{ m s}^{-1}$ .

[43] The 2011 positive GJ case sounding at 0 UTC on 17 April had a melting level and tropopause height of 3.8 and

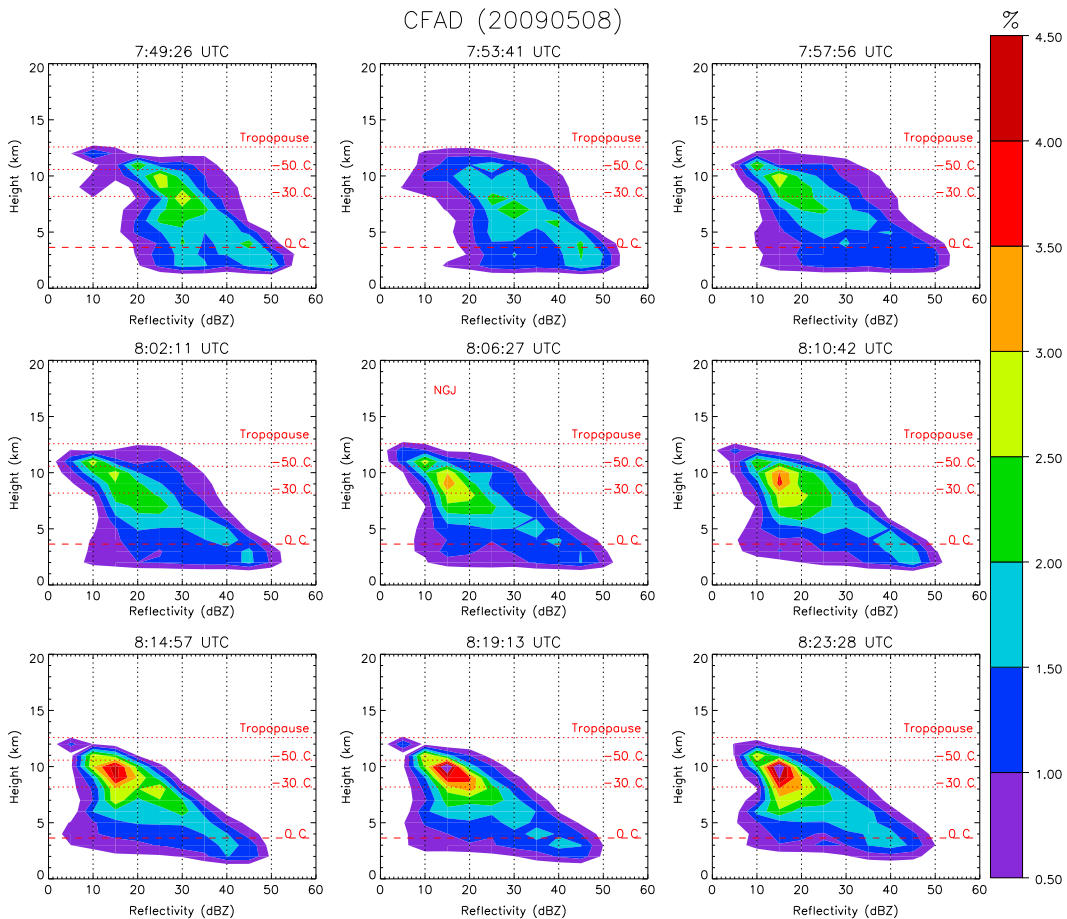


**Figure 18.** CFAD plots showing the normalized distribution of reflectivity in 5 min bins versus height for nine time steps around the time of the negative North Carolina jet. “NGJ” is labeled in the diagram when the jet occurred.

12.9 km, respectively. CAPE value was  $\sim 2300 \text{ J kg}^{-1}$ , and LI was  $-6.4$ . Precipitable water was  $36.6 \text{ kg m}^{-2}$ , the lowest of all cases but still typical of the tropics [Zveryaev and Chu, 2003]. Meanwhile, wind shear was strongest of all the cases:  $\sim 25 \text{ m s}^{-1}$ . The storm itself moved  $\sim 20 \text{ m s}^{-1}$  toward the east. In summary, the soundings from both of these days suggested favorable environments for thunderstorm formation, and the atmosphere was very moist, reminiscent of tropical air masses.

### 3.4.3. Results

[44] The storm from which the negative GJ initiated was an isolated storm, the largest in the immediate area (Figure 15). Thus, despite the ambiguity in jet position, it was clear that this storm had produced it. The 2009 negative GJ cell was about 110 km away from the KMHX radar. The vertical cross-section along the camera azimuth does not show an obvious overshooting top for this case, although there is a broad region of elevated echo tops along the 20–28 km range interval (Figure 15). The maximum reflectivity in this storm was 62 dBZ about 15 min before the jet. The 10 dBZ contour reached 14 km MSL, but this occurred  $\sim 30$  min prior to the GJ. Storm echo tops were about 2 km lower at the time of the jet, as can be seen in Figure 15. Similar to the Puerto Rico case, the location uncertainty does not allow the ability to ascertain the exact proximity of the jet relative to the coldest cloud tops. However, the infrared satellite imagery (not shown) showed that the minimum cloud top temperatures were near  $-60^\circ\text{C}$ . The most likely time of occurrence for

overshooting tops, based on interpretation of the satellite data, was 30–45 min prior to the GJ. Based on qualitative analysis of the satellite data, the storm’s anvil expanded horizontally at a roughly constant rate during the analysis period.

[45] The 2011 positive GJ storm is shown in Figure 16. The positive jet originated from a squall line moving off the coast. The storm was about 90 km from the KMHX radar. There was a small region of 15–20 dBZ above the local tropopause which indicated an overshooting top along the azimuth of the jet. This storm had a peak reflectivity value of 62 dBZ with 10 dBZ echo tops at 16 km MSL. Based on its azimuth and the location of CG activity immediately beforehand, the jet likely occurred very near the coldest IR cloud-top temperatures in the storm, which were approximately  $-70^\circ\text{C}$  (Figure 17). Note the V-shaped structure in the cold cloud of this storm, which encompasses a warmer interior east of it. U-shapes, V-shapes, and rings in cold cloud structure sometimes occur in storms producing overshooting tops, with the V-shape more likely when wind shear is strong [Setvak et al., 2010]. Based on qualitative analysis of the satellite data, the storm’s anvil expanded horizontally at a roughly constant rate during the analysis period.

[46] Since there are no LMA networks in North Carolina, 3D lightning analysis was not possible. The CFAD plots for the negative jet showed different results compared to the previous cases (Figure 18). There was a small maximum in frequency of 35 dBZ values present between the  $-30^\circ\text{C}$

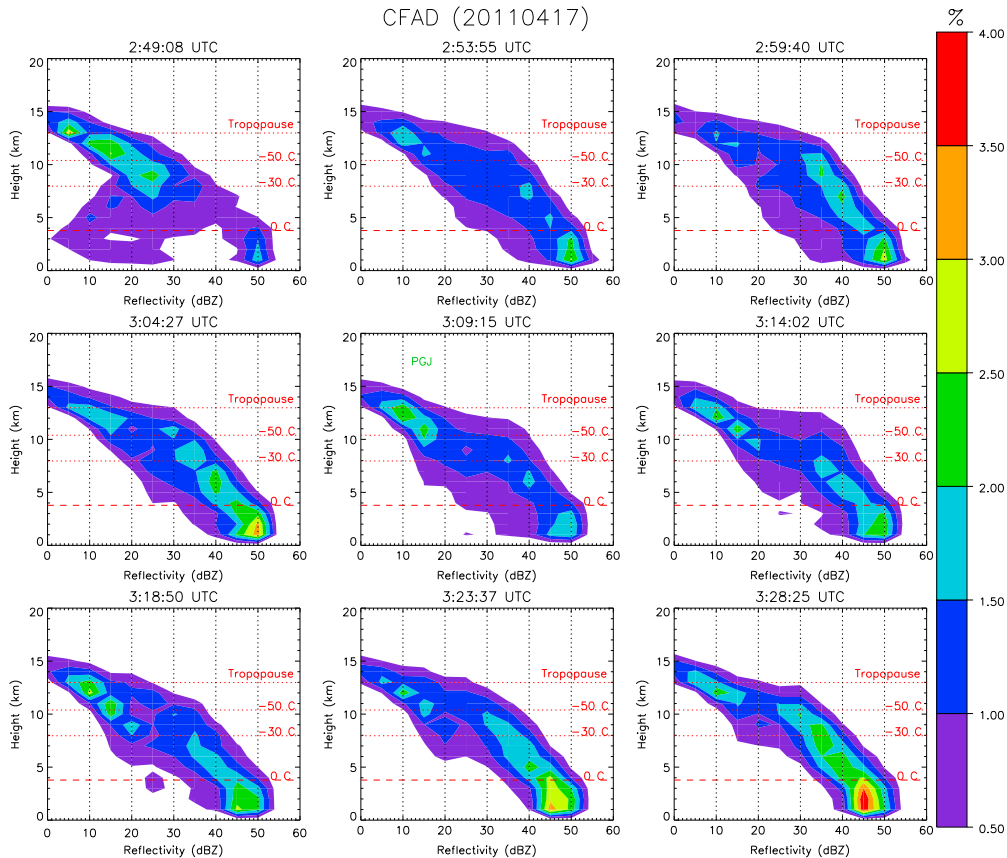


**Figure 19.** CFAD plots showing the normalized distribution of reflectivity in 5 min bins versus height for nine time steps around the time of the North Carolina positive jet. “PGJ” is labeled in the diagram when the jet occurred.

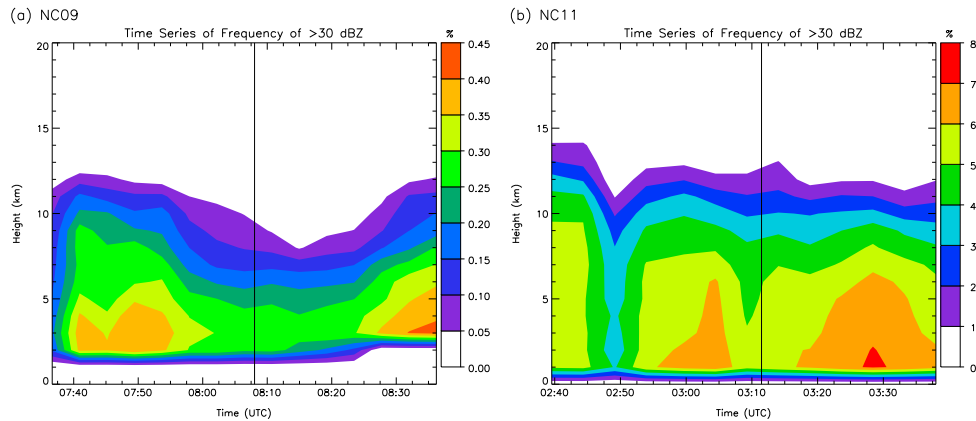


**Figure 20.** Time series plots of the frequency of  $>30$  dBZ versus height in 1 km levels with the jet time denoted by the black vertical line for (a) 8 May 2009 (negative GJ) and (b) 17 April 2011 (positive GJ).

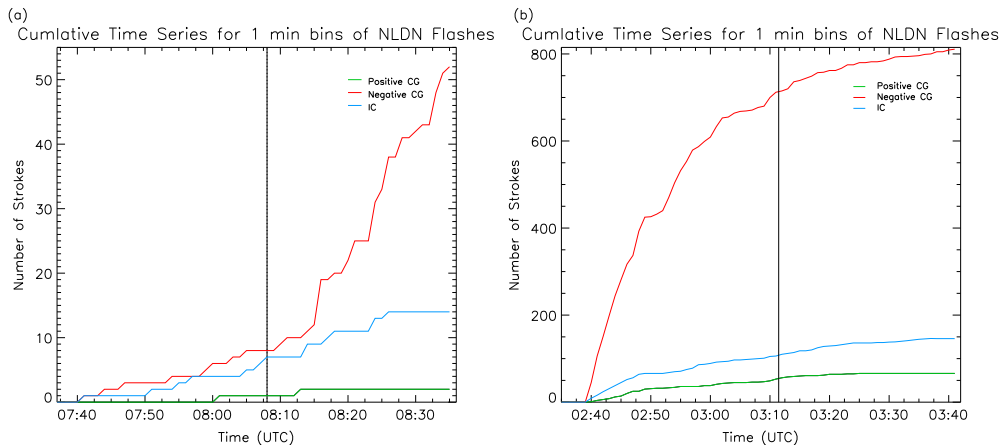


**Figure 21.** (a) Cumulative time series plot of NLDN lightning flashes in 1 min bins for the negative North Carolina jet storm. Positive CGs (green), negative CGs (red), and ICs (blue) are plotted with the time of the GJ (vertical line). (b) Same as (a) but for the positive North Carolina jet storm.

and  $-50^{\circ}\text{C}$  isotherms in the first frame, but this decreased leading up to the time of the jet, suggesting the storm was weakening. However, the frequency of 10–20 dBZ values in the upper levels continued to increase throughout the whole time period, possibly suggesting a broadening anvil. The CFADs in the positive jet case more closely resembled those in the previous cases (Figure 19). A maximum in frequency of 30–40 dBZ values at high altitudes became more prominent leading up to the time of the jet. By the time of the last frame, the maximum frequency was in the lower 5 km, indicating that the storm was raining out and weakening.

[47] A time series of reflectivity for the 2009 negative GJ case is consistent with the CFADs (Figure 20a). Unlike all the other cases, the reflectivity frequency in the upper levels was at a minimum near the time of the jet. There was also a minimum in low-level reflectivity frequency around the time of the jet which was similar to the previous cases. The time series reflectivity for the 2011 positive GJ case shows a fairly flat maximum height for 30 dBZ echo or greater, except for a small peak within the 5 min period after the jet (Figure 20b). However, reflectivity frequencies at lower altitudes were more

dynamic, with the jet occurring between two surges in frequency of 30+ dBZ below about 7 km MSL.

[48] The NLDN time series for the North Carolina cases are shown in Figure 21. Only flash data were accessible for this case. The majority of the flashes were negative CGs, and overall, very little NLDN-detected IC and positive CG lightning was noted. The 2009 negative GJ case had a lull in all lightning leading up to the time of the jet and then the negative CG lightning picked up afterward (Figure 21a). This negative CG pattern is similar to that of the Oklahoma and Florida cases. The positive jet case had a lot of negative CG activity in the beginning of the analysis, which then leveled off through the time of jet occurrence (Figure 21b).

#### 4. Conclusions

[49] The radar and lightning characteristics of five different thunderstorms that produced a total of six GJs have been examined. Table 2 shows a summary of these cases along with some of their storm characteristics. Three of them were near VHF lightning mapping networks. The Oklahoma case formed in remnants of Tropical Storm Hermine, with typical

tropical cyclone environmental characteristics such as high amounts of moisture. The Florida, Puerto Rico, and North Carolina storms formed in moist environments with high CAPE and negative LI values. The Oklahoma and Puerto Rico GJs were located over land, and the Florida and North Carolina cases occurred over water. No obvious or systematic land/water differences between the cases were apparent in environmental parameters or storm characteristics. By comparison, the multi-GJ storm studied by *Soula et al.* [2011] also developed in a very moist environment with elevated CAPE.

[50] The maximum reflectivity in the observed cases ranged from 54 to 62 dBZ, with 10 dBZ echo tops greater than 14 km MSL in all storms. Five out of the six cases featured what appeared to be overshooting tops in the radar data around the time of the jets, whether those tops broke through the sounding-defined tropopause. Temporal behavior of reflectivity in five of the six cases supported the notion of storms being near peak reflectivity height and/or vertical intensity around the times of the jets, indicating the storms were undergoing or had just passed the peak of a convective surge. Infrared satellite data, when the locations of GJs could be pinpointed, showed the GJs as occurring near the coldest cloud tops, though cloud-top temperature varied substantially between the different storms. By comparison, the GJ-producing storm studied by *van der Velde et al.*, 2007a featured 40 dBZ echoes as high as 12–15 km, with echo tops up to 17–20 km. Thus, the storms in the present study, though tall and intense, are not the tallest or strongest storms to have produced a GJ.

[51] The Oklahoma and Florida cases were marked by frequent high-altitude lightning as determined by VHF mapping networks, leading up to the time of the jets. The lightning decreased afterwards. All storms produced more negative than positive CG lightning during the 1 h analysis times that encompassed the jets. Sometimes negative CG lightning mainly occurred prior to the jets (North Carolina positive GJ), and sometimes it mainly increased afterward (Oklahoma, Florida, North Carolina negative GJ). In the Puerto Rico case, negative CGs were produced in the greatest numbers around the time of the GJ, although the overall number of strokes was small. The Puerto Rico result is most similar to the observations of *Soula et al.* [2011], who found rapid changes in lightning flash rate to occur during the GJ-producing times of one thunderstorm. Regardless, the negative CG dominance, as well as the presence of upper level VHF source maxima when those observations were available, indicates that most likely all the jet-producing storms were normal polarity [*Lang and Rutledge*, 2011]. This was confirmed by *Lu et al.* [2011b] for the Oklahoma and Florida storms via more detailed flash analysis.

[52] The observations suggest a potential link between convective surges and the occurrence of gigantic jets. *Riousset et al.* [2010] offered a physical mechanism for why this might be the case. Using a simplified model, they found that strong mixing of upper positive charge and negative screening charge could lead to electrodynamic conditions favoring the generation of a GJ. *Riousset et al.* [2010] suggested that such mixing could occur near overshooting tops or other areas of strong turbulence in the upper levels of a cloud. The present observations tend to support *Riousset et al.* [2010], since convective surges and

overshooting tops were so closely associated with the occurrence of most GJs. However, some caution needs to be exercised, for a couple reasons. The first is that very little is understood about the behavior of thundercloud charge regions in the turbulent upper levels of a convectively surging thunderstorm, and the relative roles of turbulent mixing, advective displacement, *in situ* charging, frequent lightning, and other processes—in either depleting or enhancing regions of net charge—are not well quantified. Modeling studies like *Krehbiel et al.* [2008] and *Riousset et al.* [2010] provide a useful framework for interpreting the present observational results, but they do not provide the last word on the matter.

[53] The second caveat is the case of the negative North Carolina jet, which occurred as the strongest reflectivities decreased in altitude and the storm weakened, and occurred more than 20 min past the time of peak vertical development. This was not consistent with the other cases, and thus, gigantic jets are not exclusive to times near the peak of a convective surge. Without 3D lightning information, it is difficult to say with any certainty what was truly different about this particular case. Future modeling efforts will need to account for the ability of GJs to occur under different circumstances than just convective surges.

[54] One interesting observation is the North Carolina storm that produced the positive GJ. This storm appeared to be normal polarity. *Krehbiel et al.* [2008] suggested that inverted storms, with positive charge in middle levels, would be the likely producers of positive GJs, and not normal polarity thunderstorms. There are a couple possible explanations for this unexpected behavior. One is that the thunderstorm was undergoing an overall rapid decline in negative CG rate through the time of the jet, with  $-CG$  rates then less than a third of what they were 30 min earlier. This observation was similar to *van der Velde et al.* [2007a] and may have indicated that a major shift in thunderstorm charge structure was occurring, one that potentially may have favored the production of a positive GJ. The second possibility is that this was a Type II gigantic jet as described by *Chou et al.* [2010] and thus originated as a blue jet (i.e., positive leader) between the upper positive charge and negative screening layer. Clearly, both of these hypotheses would require more detailed lightning and charge observations to test. One additional note is that the positive GJ observed by *van der Velde et al.* [2010] occurred in environment of strong wind shear, similar to the present case.

[55] The meteorological regimes examined here (multicellular tropical or tropical-like convective storms) are distinctly different from those associated with most sprite-producing convective systems [*Lyons*, 2006; *Lyons et al.*, 2009]. However, these are not the only meteorological regimes in which GJs occur. For example, *van der Velde et al.* [2010] studied a GJ that occurred over relatively shallow wintertime convection. Clearly, many additional case studies of GJ-producing storms are required to resolve the ambiguities observed in this study, and to more accurately characterize the range of meteorological scenarios in which gigantic jets occur. In addition, a major question remains about the relative rarity of GJs compared to the frequency of convective surges and overshooting tops. This would require extensive analysis of null cases (i.e., storms with unobstructed camera observations but no GJ

production) to answer, suggesting a fruitful avenue for future GJ research.

[56] **Acknowledgments.** This work was supported by the DARPA Nimbus program. The authors thank Vaisala, Inc. for providing the NLDN and GLD360 data used in this study. Without the observations of the gigantic jets, this study would not have been possible. The Florida, Oklahoma, and Puerto Rico gigantic jets were observed by Joel Gonzalez in Florida, by Kevin Palivec in Texas, and by Frankie Lucena in Puerto Rico, respectively. The authors thank the editors and reviewers of this manuscript for their assistance in improving it.

## References

- Biagi, C. J., K. L. Cummins, K. E. Kehoe, and E. P. Krider (2007), National Lightning Detection Network (NLDN) performance in southern Arizona, Texas, and Oklahoma in 2003–2004. *J. Geophys. Res.*, *112*, doi:10.1029/2006JD007341.
- Boyd, B. F., W. P. Roeder, D. Hajek, and M. B. Wilson (2005), Installation, upgrade, and evaluation a short baseline cloud-to-ground lightning surveillance system in support of space launch operations, *1st Conference on Meteorological Applications of Lightning Data*, 9–13, Jan 05, 4 pp.
- Chou, J. K., et al. (2010), Gigantic jets with negative and positive polarity streamers, *J. Geophys. Res.*, *115*, A00E45, doi:10.1029/2009JA014831.
- Chou, J. K., L. Y. Tsai, C. L. Kuo, Y. J. Lee, C. M. Chen, A. B. Chen, H. T. Su, R. R. Hsu, P. L. Chang, and L. C. Lee (2011), Optical emissions and behaviors of the blue starters, blue jets, and gigantic jets observed in the Taiwan transient luminous event ground campaign, *J. Geophys. Res.*, *116*, A07301, doi:10.1029/2010JA016162.
- Cummer, S. A., et al. (2009), Quantification of the troposphere to ionosphere charge transfer in a gigantic jet, *Nat. Geosci.*, *2*, 617–620, doi:10.1038/ngeo607.
- Cummins, K. L., Krider, E. P., Malone, M. D. (1998), The U.S. national lightning detection network and applications of cloud-to-ground lightning data by electric power utilities. *IEEE Trans. Electromagn. Compat.*, *40*(4), 465–480.
- Cummins, K. L., and M. J. Murphy (2009), An overview of lightning location systems: History, techniques, and data uses, with an in-depth look at the U.S. NLDN, *IEEE Trans. Electromagn. Compat.*, *51*(3), 499–518.
- Demetriades, N. W. S., M. J. Murphy, and J. A. Cramer (2010), Validation of Vaisala's Global Lightning Dataset (GLD360) over the continental United States. Preprints, *29th Conf. Hurricanes and Tropical Meteorology*, May 10–14, Tucson, AZ, 6 pp.
- Holle, R. (2009), [http://www.srh.noaa.gov/media/abq/sswhm/Holle\\_sw\\_hydromet\\_09.pdf](http://www.srh.noaa.gov/media/abq/sswhm/Holle_sw_hydromet_09.pdf).
- Hondl, K. D. (2003), Capabilities and components of the Warning Decision Support System-Integrated Information (WDSS-II), Preprints, *19th Conf. on Interactive Information Processing Systems (IIPS) for Meteorology, Oceanography, and Hydrology*, Long Beach, CA, Amer. Meteor. Soc., CD-ROM, 14.7.
- Hsu, R., et al. (2004), Transient luminous jets recorded in the Taiwan 2004 TLE campaign, *Eos Trans. AGU*, *85*(47), Fall Meet. Suppl., Abstract AW31a-0151.
- Krehbiel, P. R., J. A. Riousset, V. P. Pasko, R. J. Thomas, W. Rison, M. A. Stanley, and H. E. Edens (2008), Upward electrical discharges from thunderstorms, *Nat. Geosci.*, *1*, 233–237, doi:10.1038/ngeo162.
- Krehbiel, P. R., R. J. Thomas, W. Rison, T. Hamlin, J. Harlin, and M. Davis (2000), GPS-based mapping system reveals lightning inside storms, *Eos Trans. AGU*, *81*(3), 21–21, 10.1029/00EO00014.
- Lang, T. J., J. Li, W. A. Lyons, S. A. Cummer, S. A. Rutledge, and D. R. MacGorman (2011), Transient luminous events above two mesoscale convective systems: Charge moment change analysis, *J. Geophys. Res.*, *116*, A10306, doi:10.1029/2011JA016758.
- Lang, T. J., W. A. Lyons, S. A. Rutledge, J. D. Meyer, D. R. MacGorman, and S. A. Cummer (2010), Transient luminous events above two mesoscale convective systems: Storm structure and evolution, *J. Geophys. Res.*, *115*, A00E22, doi:10.1029/2009JA014500.
- Lang, T. J., S. A. Rutledge 2011, A framework for the statistical analysis of large radar and lightning datasets: Results from STEPS 2000, *Mon. Wea. Rev.*, *139*, 2536–2551.
- Lakshmanan, V., T. Smith, K. Hondl, G. J. Stumpf, and A. Witt (2006), A real-time, three dimensional, rapidly updating, heterogeneous radar merger technique for reflectivity, velocity, and derived products, *Wea. Forecasting*, *21* (5), 802–823.
- Lakshmanan, V., T. Smith, G. Stumpf, and K. Hondl. (2007), The Warning Decision Support System-Integrated Information, *Wea. And Forecasting*, *22*, 596–612.
- Lennon, C. and L. Maier, (1991), Lightning mapping system. *1991 Int'l. Aerospace and Ground Conf. on Lightning and Static Elec.*, NASA Conf. Pub. 3106, paper 89-1.
- Lu, G. et al. (2011a), Analysis of lightning development associated with gigantic jets, American Geophysics Union (AGU) Fall Meeting Abstracts, AE13B-02, 2011 December, San Francisco, United States.
- Lu, G., et al. (2011b), Lightning development associated with two negative gigantic jets, *Geophys. Res. Lett.*, *38*, L12801, doi: 10.1029/2011GL047662.
- Lu, G., S. A. Cummer, R. J. Blakeslee, S. Weiss, and W. H. Beasley (2012), Lightning morphology and impulse charge moment change of high peak current negative strokes, *J. Geophys. Res.*, *117*, D04212, doi:10.1029/2011JD016890.
- Lyons, W. A. (2006), The meteorology of transient luminous events—An introduction and overview, in NATO Advanced Study Institute on Sprites, Elves and Intense Lightning Discharges, edited by M. Fullekrug et al., pp. 19–56, Springer, New York.
- Lyons, W. A., T. E. Nelson, R. A. Armstrong, V. P. Pasko, and M. A. Stanley (2003), Upward electrical discharges from the tops of thunderstorms, *Bull. Amer. Meteor. Soc.*, *84*, 445–454.
- Lyons, W. A., M. A. Stanley, J. D. Meyer, T. E. Nelson, S. A. Rutledge, T. L. Lang, and S. A. Cummer 2009, The meteorological and electrical structure of TLE-producing convective storms, in *Lightning: Principles, Instruments and Applications*, H. D. Betz et al. (eds), pp 389–417, Springer Science + Business Media B.V., doi: 10.1007/978-1-4020-9079-017.
- MacGorman, D. R., D. W. Burgess, V. Mazur, W. D. Rust, W. L. Taylor, and B. C. Johnson 1989, Lightning rates relative to tornadic storm evolution on 22 May 1981, *J. Atmos. Sci.*, *46*, 221–250.
- MacGorman, D. R., et al. (2008), TELEX: The thunderstorm electrification and lightning experiment, *Bull. Am. Meteorol. Soc.*, *89*, 997–1013, doi:10.1175/2007BAMS2352.1.
- MacGorman, D. R., and K. E. Nielsen (1991), Cloud-to-ground lightning in a tornadic storm on 8 May 1986, *Mon. Wea. Rev.*, *119*, 1557–1574.
- Maier, L., C. Lennon, T. Britt, and S. Schaefer (1995), LDAR system performance and analysis, *International Conference on Cloud Physics*, Amer. Meteorol. Soc., Dallas, TX.
- Marshall, T. C., et al. (2005), Observed electric fields associated with lightning initiation, *Geophys. Res. Lett.* *32*, L03813.
- Mohr, C. G., and R. L. Vaughn (1979), An economical approach for Cartesian interpolation and display of reflectivity factor data in three-dimensional space, *J. Appl. Meteor.*, *18*, 661–670.
- Murphy, M. J., K. L. Cummins, N. W. S. Demetriades, and W. P. Roeder (2008), Performance of the new Four-Dimensional Lightning Surveillance System (4DLSS) at the Kennedy Space Center/Cape Canaveral Air Force Station Complex, *13th Conference on Aviation, Range, and Aerospace Meteorology*, Amer. Meteorol. Soc., Boston, MA.
- Orville, R. E. (2008), Development of the National Lightning Detection Network, *Bull. Amer. Meteorol. Soc.*, *89*(2), 180.
- Pasko, V. P., and J. J. George (2002), Three-dimensional modeling of blue jets and blue starters, *J. Geophys. Res.*, *107*(A12), 1458, doi:10.1029/2002JA009473.
- Pasko, V. P., M. A. Stanley, J. D. Mathews, U. S. Inan, and T. G. Wood (2002), Electrical discharge from a thundercloud top to the lower ionosphere, *Nature*, *416*, 152–154, doi:10.1038/416152a.
- Riousset, J. A., V. P. Pasko, P. R. Krehbiel, W. Rison, and M. A. Stanley (2010), Modeling of thundercloud screening charges: Implications for blue and gigantic jets, *J. Geophys. Res.*, *115*, A00E10, doi:10.1029/2009JA014286.
- Rison, W., R. J. Thomas, P. R. Krehbiel, T. Hamlin, and J. Harlin (1999), A GPS-based three-dimensional lightning mapping system: Initial observations in central New Mexico, *Geophys. Res. Lett.*, *26*(23), 3573–3576.
- Roeder, W. P. (2010), The four dimensional lightning surveillance system, *21st International Lightning Detection Conference*, Vaisala, Orlando, Fla.
- Said, R. K., U. S. Inan, and K. L. Cummins (2010), Long-range lightning geo-location using a VLF radio atmospheric waveform bank, *J. Geophys. Res.*, *115*, D23108, doi:10.1029/2010JD013863.
- Setvak, M. et al. (2010), Satellite-observed cold-ring-shaped features atop deep convective clouds, *Atmos. Res.*, *97*, 80–96.
- Soula, S., O. van der Velde, J. Montanya, P. Huet, C. Barthe, and J. Bór (2011), Gigantic jets produced by an isolated tropical thunderstorm near Réunion Island, *J. Geophys. Res.*, *116*, D19103, doi:10.1029/2010JD015581.
- Su, H. T., et al. (2003), Gigantic jets between a thundercloud and the ionosphere, *Nature*, *423*, 974–976, doi:10.1038/nature01759.
- van der Velde, O. A., J. Bor, J. Li, S. A. Cummer, E. Arnone, F. Zanotti, M. Fullekrug, C. Haldoupis, S. NaitAmor, and T. Farges (2010), Multi-instrumental observations of a positive gigantic jet produced by a winter thunderstorm in Europe, *J. Geophys. Res.*, *115*, D24301, doi:10.1029/2010JD014442.
- van der Velde, O. A., et al. (2007a), Analysis of the first gigantic jet recorded over continental North America, *J. Geophys. Res.*, *112*, D20104, doi:10.1029/2007JD008575.
- van der Velde, O. A., W. A. Lyons, S. A. Cummer, N. Jaugey, D. D. Sentman, M. B. Cohen, and R. Smedley (2007b), Electromagnetic, visual and meteorological analyses of two gigantic jets observed over Missouri. *Eos Trans AGU*, Fall Meet, Suppl., Poster, Abstract AE23A-0895.

- Wiens, K. C., Rutledge, S. A., and Tessendorf, S. A. (2005), The 29 June 2000 supercell observed during STEPS. Part II: Lightning and charge structure, *J. Atmos. Sci.*, *62*, 4151–4177.
- Wescott, E. M., Stenbaek-Nielsen, H. C., Huet, P., Heavner, M. J., and Moudry, D. R. (2001), New evidence for the brightness and ionization of blue jets and blue starters, *J. Geophys. Res.*, *106*, 21549–21554.
- Wescott, E. M., Sentman, D. D., Heavner, M. J., Hampton, D. L., and O. H. Vaughan Jr. (1998), Blue jets: Their relationship to lightning and very large hailfall, and their physical mechanisms for their production, *J. Atmos. Sol. Terr. Phys.*, *60*, 713–724.
- Williams, E. R., et al. (1999), The behavior of total lightning activity in severe Florida thunderstorms, *Atmos. Res.*, *51*, 245–264.
- Wilson, C. T. R. (1956), A theory of thundercloud electricity, *Proc. R. Soc. Lond.*, *A236*, 297–317.
- Wilson, C. T. R. (1921), Investigations on lightning discharges and on the electric field of thunderstorms, *Phil. Trans. R. Soc. Lond.*, *A221*, 73–115.
- Yuter, S. E., and R. A. Houze Jr. (1995), Three-dimensional kinematic and microphysical evolution of Florida cumulonimbus. Part II: Frequency distribution of vertical velocity, reflectivity, and differential reflectivity, *Mon. Wea. Rev.*, *123*, 1941–1963.
- Zveryaev, I. I. and P.-S. Chu (2003), Recent climate changes in precipitable water in the global tropics as revealed in National Centers for Environmental Prediction/National Center for Atmospheric Research reanalysis, *J. Geophys. Res.*, *108*(D10), 4311, doi:10.1029/2002JD002476.